



THE UNIVERSITY *of* EDINBURGH

Edinburgh Research Explorer

Thermoplastic hybrid-matrix composites prepared by a room-temperature vacuum infusion and in-situ polymerisation process

Citation for published version:

Obande, W, O Brádaigh, C & Ray, D 2020, 'Thermoplastic hybrid-matrix composites prepared by a room-temperature vacuum infusion and in-situ polymerisation process', *Composites Communications*, vol. 22, 100439. <https://doi.org/10.1016/j.coco.2020.100439>

Digital Object Identifier (DOI):

[10.1016/j.coco.2020.100439](https://doi.org/10.1016/j.coco.2020.100439)

Link:

[Link to publication record in Edinburgh Research Explorer](#)

Document Version:

Peer reviewed version

Published In:

Composites Communications

General rights

Copyright for the publications made accessible via the Edinburgh Research Explorer is retained by the author(s) and / or other copyright owners and it is a condition of accessing these publications that users recognise and abide by the legal requirements associated with these rights.

Take down policy

The University of Edinburgh has made every reasonable effort to ensure that Edinburgh Research Explorer content complies with UK legislation. If you believe that the public display of this file breaches copyright please contact openaccess@ed.ac.uk providing details, and we will remove access to the work immediately and investigate your claim.



1 **Thermoplastic hybrid-matrix composites prepared by a room-** 2 **temperature vacuum infusion and in-situ polymerisation process**

3 Winifred Obande, Conchúr M. Ó Brádaigh, and Dipa Ray*

4 School of Engineering, Institute for Materials and Processes, The University of Edinburgh,
5 Sanderson Building, Robert Stevenson Road, Edinburgh EH9 3FB, Scotland, United Kingdom.

6 *Corresponding author. *Email address:* dipa.roy@ed.ac.uk

7 **Keywords:** Polymer-matrix composite; Hybrid matrix; Liquid thermoplastic resin; Mechanical
8 properties; Resin infusion; Fibre-reinforced composite

9 10 **Abstract**

11 This work explores a novel route for the fabrication of hybrid-matrix composites based on a recently
12 developed liquid thermoplastic acrylic resin. This liquid resin was modified using a poly(phenylene
13 ether) (PPE) oligomer with vinyl functionality. Glass fibre-reinforced laminates based on acrylic and
14 PPE-modified acrylic matrices were produced by a room-temperature vacuum infusion and in-situ
15 polymerisation process. Comparative assessments of their mechanical performance and mode-I
16 interlaminar fracture behaviour revealed enhanced matrix ductility, transverse flexural properties
17 and initiation fracture toughness. Crazeing was identified as the dominant mechanism for improved
18 resistance to crack initiation.

19 **1 Introduction**

20 Innovative low-viscosity liquid thermoplastic (LTP) resins can readily infiltrate into fibrous
21 reinforcement under conditions of relatively low temperature and pressure in the same way
22 that thermoset (TS) resins can [1–4]. Room-temperature infusible acrylic resins with
23 viscosities as low as 100 mPa.s have received considerable research attention in recent years
24 [5–13]. In our previous work, we presented comparisons between the mechanical
25 performance of acrylic composites with equivalent epoxy composites and reported inferior
26 transverse flexural performance [7] and impact damage resistance [8] in the acrylic-matrix
27 composites.

28 Structural composites typically comprise a thermoset matrix or a semi-crystalline
29 thermoplastic matrix. Cross-linked networks and crystalline domains contribute to enhanced
30 matrix rigidity, making them ideal candidates for high-performance applications. In contrast,
31 purely amorphous matrices such as acrylics do not contain cross-links or crystalline regions
32 within their molecular structure. Thus, this might influence composite properties,
33 particularly when matrix strength plays a key role.

1 Therefore, there is a significant scope to tailor the structure of acrylic-matrix composites for
2 enhanced performance under different loading conditions. Recent works on this topic have
3 used Nanostrength™ triblock copolymers comprising polymethylmethacrylate-b-
4 polybutylacrylate-b-polymethylmethacrylate [9–11] and hybrid fibre reinforcements [12] to
5 realise improved composite properties. However, TP-TP hybridisation of an acrylic matrix,
6 via in-situ polymerisation, is novel and never investigated before.

7 Poly(phenylene ether) (PPE) – an amorphous engineering thermoplastic, is arguably one of
8 the most successfully applied as a modifier in TS-matrix composites [14–16]. Unlike the
9 acrylic matrix, which is a purely aliphatic amorphous TP, PPE contains aromatic rings, which
10 may confer some rigidity in a hybrid system and is thus, worthy of exploration.

11 This present study investigates an innovative route to obtaining vacuum-infusible hybrid-
12 matrix composites based on acrylic and PPE. To promote reactive blending during in-situ
13 polymerisation of the hybrid matrix, PPE with vinyl functionality was selected for this study.
14 The effects of hybridisation on mechanical and morphological properties are presented
15 herein.

16 **2 Experimental**

17 **2.1 Materials and fabrication**

18 Two 4-mm thick (nominally) test laminates were prepared by a room-temperature vacuum
19 infusion and in-situ polymerisation process. Table 1 provides an overview of the materials
20 used. Full details of the materials and the fabrication processes used are supplied in Appendix
21 A.

Table 1. Summary of materials used for composite fabrication.

	<i>Elium</i> [®] 188 O ^a	<i>NORYL</i> [™] SA9000 ^b	<i>Q-UD Glass</i> ^c
<i>Unreinforced polymer samples</i> ^d			
<i>A100/P0</i>	100	0	0
<i>A95/P5</i>	95	5	0
<i>Composite samples</i> ^d			
<i>GF/A100/P0</i>	100	0	50
<i>GF/A95/P5</i>	95	5	57

^a A Liquid acrylic resin [A] supplied by Arkema GRL, France.
^b An oligomeric PPE resin [P] with vinyl functionality, supplied by SABIC.
^c TEST2594 – a quasi-unidirectional (UD) glass non-crimp fabric (NCF) supplied by Ahlstrom-Munksjö. GF: glass fibre. Fibre volume fraction.
^d Polymerised using a dibenzoyl peroxide initiator – BP50FT supplied by United Initiators.

2.2 Mechanical and thermomechanical characterisation

2.2.1 Tensile testing

Tensile properties were evaluated in accordance with ASTM D3039 under transverse tension.

2.2.2 Short beam shear testing

Short beam shear properties were evaluated by short beam shear testing using a span-to-thickness ratio of 4:1 in accordance with ASTM D2344.

2.2.3 Flexural testing

Non-standard flexural testing was performed on unreinforced matrix samples as detailed in Appendix B. To gain further insights on differences in fracture behaviour of the matrices, SEM inspections were also performed.

Flexural properties of glass fibre-reinforced composite samples were determined by three-point bending (ASTM D7264 – Procedure A) using a span-to-thickness ratio of 32:1 under longitudinal and transverse loading.

2.2.4 Mode-I interlaminar fracture toughness (ILFT) testing

Mode-I ILFT was evaluated using double cantilever beam tests per ASTM D5528. SEM inspections were conducted on DCB fracture surfaces to assess fracture behaviour.

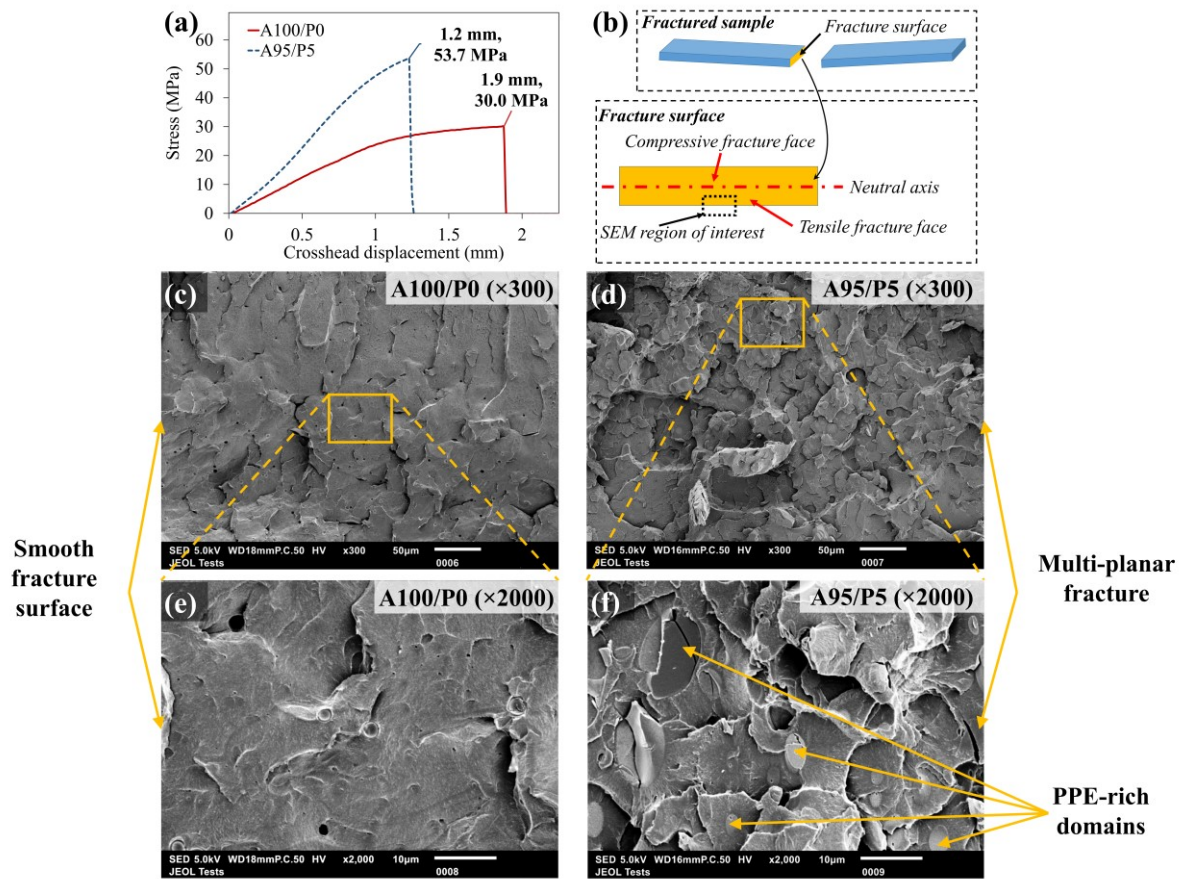
The interested reader is referred to Appendix B for supplementary specimen and test specifications.

1 **3 Results and discussions**

2 3.1 Flexural test results of unreinforced matrices

3 PPE modification appears to improve flexural strength and stiffness of the GF/A95/P5
4 sample as evidenced by the stress-displacement curves in Figure 1(a). Although mid-span
5 deflections were not measured during testing, the observed increase in stiffness may
6 tentatively indicate an increase in modulus. These results are based on single-sample tests
7 and are thus, not conclusive. These results provide interesting insights, however, that are
8 worthy of further investigation.

9 The micrographs from the regions of interest, diagrammatically shown in Figure 1(b), reveal
10 relatively flat fracture topography for A100/P0 (Figure 1(c)), and multi-planar fractures for
11 the A95/P5 matrix (Figure 1(d)), which suggests an interplay of crack deflection and crack
12 penetration mechanisms as detailed in Appendix C [17]. At higher magnifications, the
13 A100/P0 matrix appears homogenous (Figure 1(e)); a biphasic morphology comprising
14 discrete domains was observed for the A95/P5 matrix (Figure 1(f)). These domains are likely
15 PPE-rich phase, surrounded by an acrylic-rich phase.



1
2 *Figure 1. Flexural stress-displacement curves (a) and diagrammatic representation of the*
3 *SEM region of interest (b). SEM micrographs of fracture surfaces of unreinforced (c) & (e)*
4 *A100/Po and (d) & (f) A95/P5 samples at different magnifications (×300 & ×2000).*

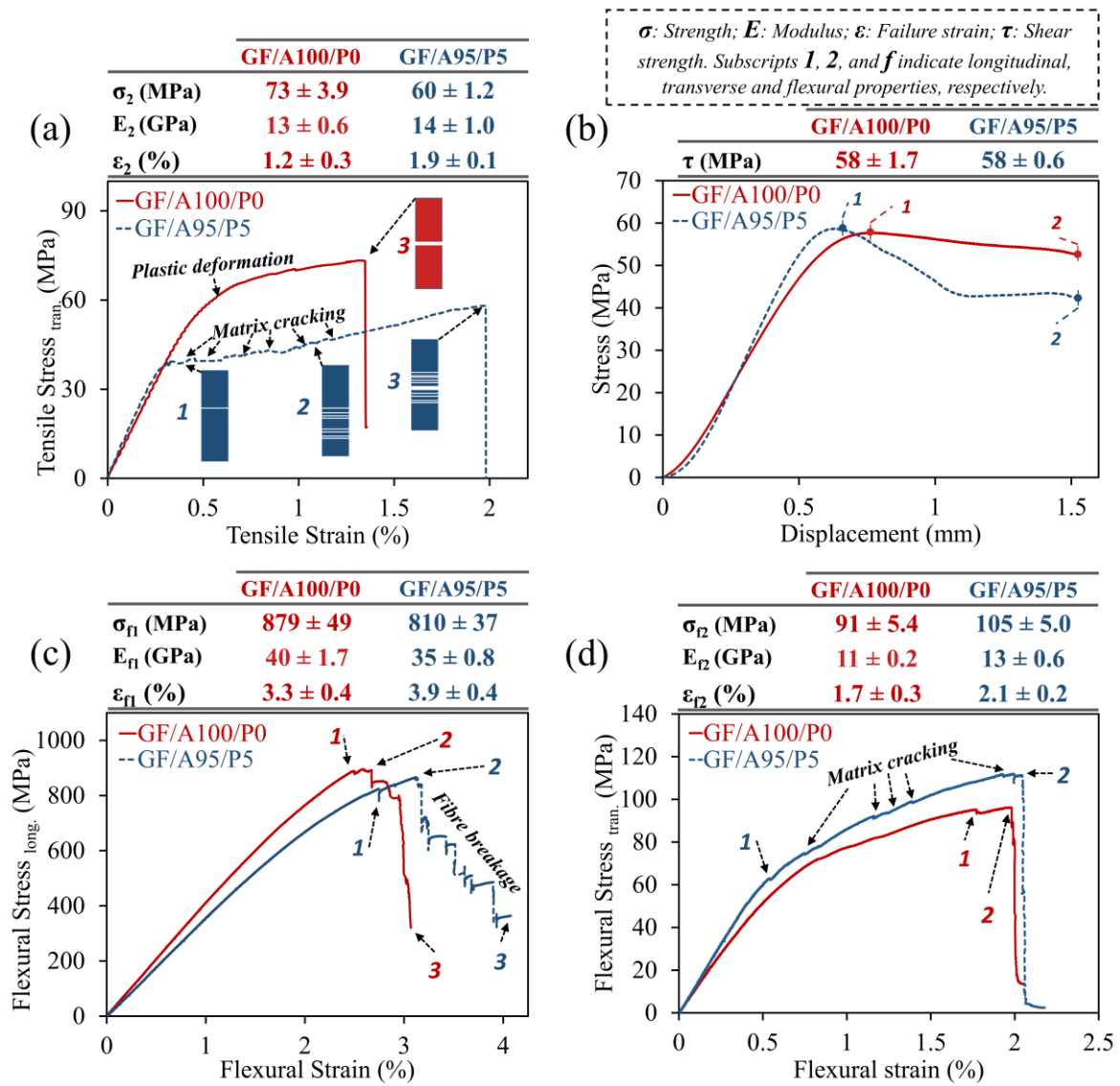
5 3.2 Results of composites testing

6 3.2.1 Transverse tensile test results

7 Representative stress-strain responses and average transverse tensile strengths, moduli and
8 failure strains of the GF/A100/Po and GF/A95/P5 materials are presented in Figure 2(a).
9 Both materials exhibit similar linear behaviour initially; however, an earlier onset of damage
10 initiation (matrix cracking) was observed with the GF/A95/P5 samples. From Points 1 to 3
11 Figure 2(a), matrix crack accumulation occurs before ultimate failure. In contrast, the
12 GF/A100/Po material undergoes plastic deformation up to failure. Matrix hybridisation
13 resulted in reduced (-18%) transverse tensile strength with a slight increase in modulus
14 (+8%) and significant increases in failure strain (+58%). Thus, hybridisation appears to
15 increase both transverse composite modulus and ductility. Moreover, higher areas bounded
16 under GF/A95/P5 curves may suggest enhanced toughness.

1 **3.2.2 Short beam shear test results**

2 Figure 2(b) shows the results of short beam shear tests performed on the GF/A100/P0 and
 3 GF/A95/P5 materials. For both materials, all samples exhibited plastic deformation up to
 4 their respective ultimate shear stress values (Point 1). However, beyond this point, the curves
 5 of GF/A95/P5 samples exhibited a more abrupt loss in stiffness with increasing displacement
 6 between Points 1 and 2.



7
 8 *Figure 2. Representative curves and results for GF/A100/P0 (red) and GF/A95/P5 (blue)*
 9 *following loading in (a) transverse tension; (b) short beam shear; (c) longitudinal flexure*
 10 *and (d) transverse flexure.*

11 **3.2.3 Flexural test results**

12 Results from longitudinal flexural tests are presented in Figure 2(c). All samples of both
 13 materials exhibited a three-stage stress-strain evolution: (i) an initial linear-elastic region,
 14 (ii) a region of slight nonlinearity, and (iii) the onset of damage (Point 1). Post-peak strain

1 evolution between Points 2 and 3 was relatively more confined in GF/A100/P0 samples than
 2 in GF/A95/P5. Progressive fibre fractures over a broader range of strains may provide
 3 evidence of superior damage resistance and possibly toughness in the GF/A95/P5 material.
 4 Moreover, it exhibited markedly higher (18%) average failure strain than the GF/A100/P0.

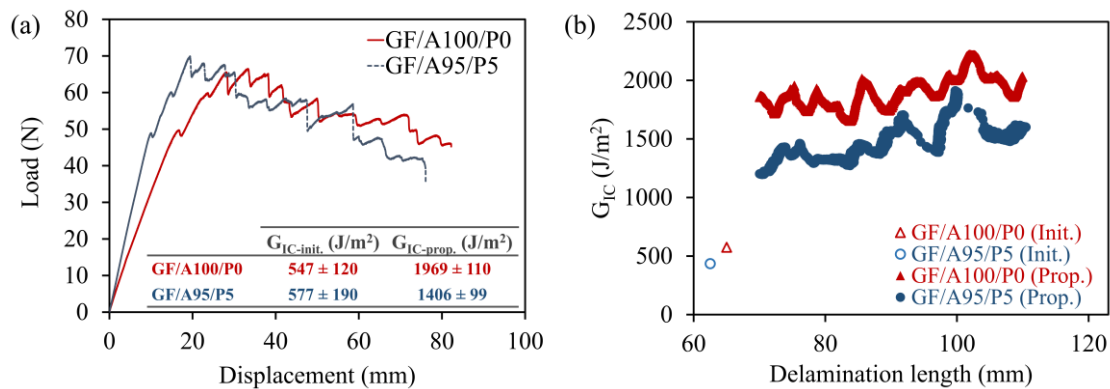
5 Hybridisation did, however, produce a laminate with lower longitudinal flexural strength (-
 6 8%) and modulus (-18%).

7 In Figure 2(d), the results of transverse flexural tests are presented. All samples across both
 8 materials exhibited an initial region of linearity, beyond which, plastic deformation ensued
 9 with a distinct onset of failure (Point 1) and abrupt ultimate failure at Point 2. All GF/A95/P5
 10 samples underwent cumulative matrix cracking in plies under tension, such as those shown
 11 between Points 1 and 2. The hybrid-matrix composite exhibited improved transverse flexural
 12 strength (+15%), modulus (+18%) and failure strain (+24%) relative to the unmodified
 13 reference.

14 Differences in the trends between the comparative transverse tensile and flexural
 15 performance were likely attributed to the sensitivity of the former to defect distribution
 16 across the gauge length. Thus, it can be concluded that hybridisation improved the composite
 17 transverse strength, modulus, ductility and overall interfacial strength.

18 3.2.4 Mode-I interlaminar fracture toughness test results

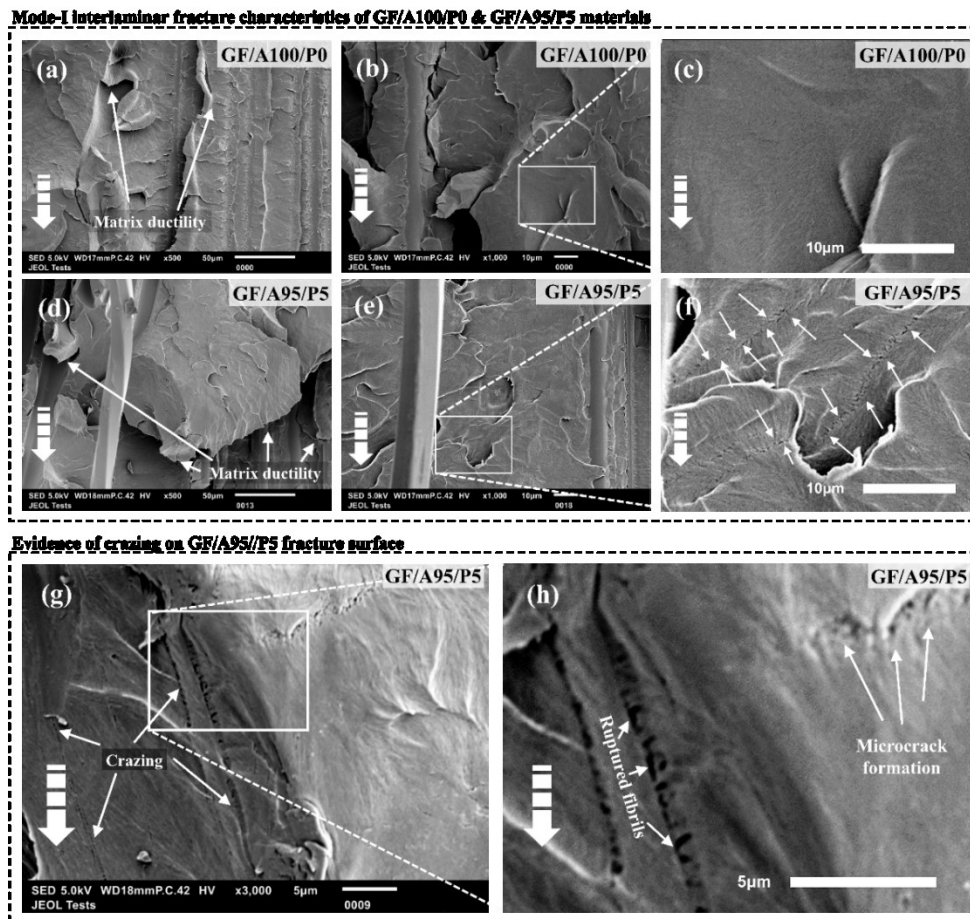
19 Representative DCB load-displacement curves and obtained results are shown in Figure 3(a).
 20 Despite exhibiting superior longitudinal flexural stiffness, GF/A100/P0 samples had
 21 unexpectedly lower crack opening stiffness up to initiation, which may be explained by a
 22 higher fibre volume fraction in the GF/A95/P5 laminate. Both materials underwent unstable
 23 crack growth due to the presence of 90° fibres within the fabric.



24
 25 *Figure 3. (a) Representative load-displacement curves and (b) R-curves for GF/A100/P0*
 26 *(red) and GF/A95/P5 (blue) following double cantilever beam testing.*

1 Hybridisation conferred a 5% increase in the initiation fracture toughness ($G_{IC-init.}$); however,
 2 propagation fracture toughness ($G_{IC-prop.}$) decreased by 29%. Similar results were reported by
 3 Lee et al. [18] who found that hybridisation only enhanced $G_{IC-init.}$, but $G_{IC-prop.}$ was reduced
 4 due to limited fibre bridging in the hybrid composite. This is supported by literature on
 5 factors affecting propagation behaviour [11,19,20]. Moreover, other factors limiting fibre
 6 bridging in the GF/A95/P5 material may be its plausibly higher matrix modulus [17]
 7 (evidenced by the higher stiffness reported in 3.1) and enhanced interfacial strength as
 8 discussed in 3.2.3 [21,22]. Interestingly, R-curves (Figure 3(b)) did not reveal discernibly
 9 distinct propagation behaviour between both materials.

10 Figure 4 (a)-(f) presents DCB fracture surfaces of GF/A100/P0 and GF/A95/P5 samples
 11 obtained using SEM. Both surfaces appear texturally coarse and dull, indicating comparable
 12 ductility on a microscopic scale.



13

14 *Figure 4. SEM micrographs showing mode-I fracture surfaces of (a), (b) & (c)*
 15 *GF/A100/P0 and (d)-(h) GF/A95/P5. The larger broken arrows show the direction of*
 16 *crack propagation. In (f), arrows highlight paths of microcrack formation.*

1 The GF/A95/P5 sample showed evidence of microcrack formation (Figure 4(f)) and multiple
2 sites of crazing (Figure 4(g)), features which were not observed for GF/A100/Po. The
3 microcracks appeared as long craze-like interpenetrating paths across the fracture surface;
4 however, no coalescence was observed at their points of intersection. Crazing is a dominant
5 plastic deformation mechanism in amorphous TP matrices [23,24], which may explain the
6 increased $G_{IC-init.}$.

7 The absence of discernible PPE-rich domains in the micrographs of the GF/A95/P5 sample
8 compared with those of the A95/P5 sample may highlight the effects of fibres on the resulting
9 phase morphology. However, further investigations would be required to substantiate this
10 hypothesis.

11 **4 Conclusions**

12 This study represents the first implementation of a novel approach for room temperature
13 vacuum infusion of continuous fibre, thermoplastic hybrid-matrix composites. The approach
14 exploits the low viscosity of liquid TP acrylic resins and with a higher performance
15 poly(phenylene ether) with vinyl functionality to realise enhanced reactivity during the in-
16 situ polymerisation processing. The following are the key observations and conclusions from
17 the benchmarking of mechanical performance with respect to an unmodified acrylic reference
18 laminate:

- 19 • **Enhanced ductility in the hybrid-matrix composite:** failure strains increased
20 under transverse tension (+58%), transverse flexure (+24%) and longitudinal flexure
21 (+18%).
- 22 • **Improved composite transverse flexural strength (+15%) and modulus**
23 **(+18%):** this may suggest enhancements in matrix strength, modulus and interfacial
24 adhesion.
- 25 • **A 5% increase in initiation fracture toughness,** possibly due to the effects of
26 multiple crazing of the hybrid matrix system.
- 27 • **Decreased propagation fracture toughness by 29%,** possibly due to diminished
28 contributions from fibre bridging.

29 The investigation of the reaction kinetics and mechanism between acrylic resin and PPE, and
30 how this relates to phase separation and morphology is recommended as future work.

1 **5 Acknowledgements**

2 The authors gratefully acknowledge Arkema GRL, France and SABIC for the provision of
3 materials and technical support towards this research. SABIC and brands marked with TM are
4 trademarks of SABIC or its subsidiaries or affiliates, unless otherwise noted.

5 **6 References**

- 6 [1] H. Parton, I. Verpoest, In situ polymerization of thermoplastic composites based on
7 cyclic oligomers, *Polym. Compos.* 26 (2005) 60–65.
- 8 [2] K. Van Rijswijk, J.J.E. Teuwen, H.E.N. Bersee, A. Beukers, Textile fiber-reinforced
9 anionic polyamide-6 composites. Part I: The vacuum infusion process, *Compos. Part A*
10 *Appl. Sci. Manuf.* 40 (2008) 1–10.
11 <https://doi.org/10.1016/j.compositesa.2008.03.018>.
- 12 [3] J.J. Murray, C. Robert, K. Gleich, E.D. McCarthy, C.M. Ó Brádaigh, Manufacturing of
13 unidirectional stitched glass fabric reinforced polyamide 6 by thermoplastic resin
14 transfer moulding, *Mater. Des.* 189 (2020) 108512.
15 <https://doi.org/10.1016/j.matdes.2020.108512>.
- 16 [4] Y. Zhao, X. Ma, T. Xu, D.R. Salem, H. Fong, Hybrid multi-scale thermoplastic
17 composites reinforced with interleaved nanofiber mats using in-situ polymerization of
18 cyclic butylene terephthalate, *Compos. Commun.* 12 (2019) 91–97.
19 <https://doi.org/10.1016/j.coco.2019.01.005>.
- 20 [5] R.E. Murray, D. Snowberg, D. Berry, R. Beach, S. Rooney, D. Swan, Manufacturing a
21 9-meter thermoplastic composite wind turbine blade, in: *Am. Soc. Compos. 32nd Tech.*
22 *Conf.*, West Lafayette, Indiana, 2017. www.nrel.gov/publications. (accessed January 1,
23 2019).
- 24 [6] D.S. Cousins, *Advanced thermoplastic composites for wind turbine blade*
25 *manufacturing*, Colorado School of Mines [Doctoral Thesis], 2018.
- 26 [7] W. Obande, D. Mamalis, D. Ray, L. Yang, C.M. Ó Brádaigh, Mechanical and
27 thermomechanical characterisation of vacuum-infused thermoplastic- and thermoset-
28 based composites, *Mater. Des.* 175 (2019) 107828.
29 <https://doi.org/10.1016/j.matdes.2019.107828>.
- 30 [8] W. Obande, D. Ray, C.M. Ó Brádaigh, Viscoelastic and drop-weight impact properties
31 of an acrylic-matrix composite and a conventional thermoset composite – A

- 1 comparative study, *Mater. Lett.* 238 (2019) 38–41.
2 <https://doi.org/10.1016/j.matlet.2018.11.137>.
- 3 [9] M.R. Boumbimba, M. Coulibaly, A. Khabouchi, G. Kinvi-Dossou, N. Bonfoh, P. Gerard,
4 Glass fibres reinforced acrylic thermoplastic resin-based tri-block copolymers
5 composites: Low velocity impact response at various temperatures, *Compos. Struct.*
6 160 (2017) 939–951. <https://doi.org/10.1016/j.compstruct.2016.10.127>.
- 7 [10] G. Kinvi-Dossou, R. Matadi Boumbimba, N. Bonfoh, S. Garzon-Hernandez, D. Garcia-
8 Gonzalez, P. Gerard, A. Arias, Innovative acrylic thermoplastic composites versus
9 conventional composites: improving the impact performances, *Compos. Struct.* 217
10 (2019) 1–13. <https://doi.org/10.1016/j.compstruct.2019.02.090>.
- 11 [11] T. Pini, Fracture behaviour of thermoplastic acrylic resins and their relevant
12 unidirectional carbon fibre composites : rate and temperature effects, Politecnico di
13 Milano [Doctoral Thesis], 2017.
- 14 [12] M.E. Kazemi, L. Shanmugam, D. Lu, X. Wang, B. Wang, J. Yang, Mechanical properties
15 and failure modes of hybrid fiber reinforced polymer composites with a novel liquid
16 thermoplastic resin, Elium®, *Compos. Part A Appl. Sci. Manuf.* 125 (2019).
17 <https://doi.org/10.1016/j.compositesa.2019.105523>.
- 18 [13] S.K. Bhudolia, S.C. Joshi, Low-velocity impact response of carbon fibre composites
19 with novel liquid methylmethacrylate thermoplastic matrix, *Compos. Struct.* 203
20 (2018) 696–708. <https://doi.org/10.1016/j.compstruct.2018.07.066>.
- 21 [14] R.W. Venderbosch, H.E.H. Meijer, P.J. Lemstra, Processing of intractable polymers
22 using reactive solvents: 1. Poly(2,6-dimethyl-1,4-phenylene ether)/epoxy resin, 1993.
- 23 [15] R.W. Venderbosch, H.E.H. Meijer, P.J. Lemstra, Processing of intractable polymers
24 using reactive solvents. 2. poly(2,6-dimethyl-1,4-phenylene ether) as a matrix material
25 for high-performance composites, *Polymer (Guildf)*. 36 (1995) 1167–1178.
26 [https://doi.org/10.1016/0032-3861\(95\)93918-C](https://doi.org/10.1016/0032-3861(95)93918-C).
- 27 [16] H. Cong, B. Yu, H. Yuan, C. Tian, S. Yang, Preparation and characterization of
28 nanocomposites with polyphenylene oxide, in: V. Mittal (Ed.), *Manuf. Nanocomposites*
29 with Eng. Plast., Woodhead Publishing, 2015.
- 30 [17] Q. Zhang, S. Liang, G. Sui, X. Yang, Influence of matrix modulus on the mechanical and
31 interfacial properties of carbon fiber filament wound composites, *RSC Adv.* 5 (2015)
32 25208–25214. <https://doi.org/10.1039/c5ra00098j>.

- 1 [18] J.J. Lee, S.L. Ogin, P.A. Smith, Interlaminar fracture toughness of glass fiber laminates
2 additionally reinforced with carbon bead, in: ASTM Spec. Tech. Publ., 1995.
3 <https://doi.org/10.1520/stp14007s>.
- 4 [19] T. Pini, F. Briatico-Vangosa, R. Frassine, M. Rink, Matrix toughness transfer and fibre
5 bridging laws in acrylic resin based CF composites, Eng. Fract. Mech. 203 (2018) 115–
6 125. <https://doi.org/10.1016/j.engfracmech.2018.03.026>.
- 7 [20] P. Compston, P.B. Jar, The Transfer of Matrix Toughness to Composite Mode I
8 Interlaminar Fracture Toughness in Glass-Fibre / vinyl Ester Composites, Appl.
9 Compos. Mater. 9 (2002) 291–314.
- 10 [21] H. Ming Chong, Toughening mechanisms of block copolymer and graphene
11 nanoplatelet modified epoxy polymers, 2015.
- 12 [22] K. Masanai, Toughening mechanisms of silica nanoparticle-modified epoxy polymers,
13 Imperial College London, 2010.
- 14 [23] K.Y. Kim, L. Ye, C. Yan, Fracture behavior of polyetherimide (PEI) and interlaminar
15 fracture of CF/PEI laminates at elevated temperatures, Polym. Compos. 26 (2005) 20–
16 28. <https://doi.org/10.1002/pc.20062>.
- 17 [24] S. Pal, B.C. Ray, Molecular Dynamics Simulation of Nanostructured Materials: An
18 Understanding of Mechanical Behavior, 2020.

19